Influence of sublattice bias on superfluid to Mott insulator transitions

Akshay Sawhney* and Erich J. Mueller†
Laboratory of Atomic and Solid State Physics, Cornell University, Ithaca, New York 14853, USA

(Received 30 March 2021; accepted 7 June 2021; published 16 June 2021)

We model the superfluid to Mott insulator transition for a Bose gas on a lattice with two inequivalent sublattices. Using the Gutzwiller ansatz, we produce phase diagrams and provide an understanding of the interplay between superfluidity on each sublattice. We explore how the Mott lobes split and describe the experimental signatures.

DOI: 10.1103/PhysRevA.103.063308

I. INTRODUCTION

The most iconic experiment in cold atom physics was the observation of the superfluid to Mott insulator transition [1]. In the superfluid phase atoms are delocalized throughout the entire lattice, while in the Mott insulating phase interactions suppress atomic motion. This transition is a prototype for understanding strong correlation effects in quantum degenerate matter. In subsequent years more sophisticated experiments were developed for exploring this transition [2–14]. Of particular interest is the role of lattice geometry, which is being explored in experiments which create exotic non-Bravais lattices [15]. Here we conduct a mean-field study of interacting bosons in such lattices.

At its core the superfluid-Mott transition is a competition between kinetic energy, which favors macroscopically occupying delocalized states, and interactions, which favor product states where each site has a definite occupation. As one changes the lattice geometry, the nature of the delocalized states can change, influencing this energy balance. One extreme example of this behavior are studies of the superfluid-Mott transition in Hubbard-Hoffstadter models, which boast relatively flat bands with topological character [16–19]. Here we explore a different phenomenon, namely how the structure within a unit cell influences the transition.

Motivated by experiments at Berkeley [20], we consider the case where the lattice depth is different for two sublattices. Figure 1 shows some examples: atoms sit at the sites marked by x's and dots, but have different energies on each of these sublattices. The Berkeley experiments were restricted to the extreme cases where the energy offset was very large, and where it vanished. Our work addresses the following general problems. How does the phase diagram evolve as one changes the offset? How does this offset influence the condensate?

Technically, one creates such optical lattices by interfering laser beams. The lattice geometry is set by the intensity and wave vectors of the lasers. Experiments have demonstrated kagome, checkerboard, Lieb, striped, triangular, and honeycomb lattices [15,21–27]. Superlattice geometries, which have been used to produce ladders and plaquettes, are closely related [28,29], and similar techniques are used to produce disordered and quasiperiodic structures [30–32]. Some theoretical questions have been addressed in specific geometries [33].

We find that the interplay of superfluidity on the two lattices is quite rich: superfluidity can be suppressed on one sublattice, while remaining strong on the other. The most trivial example is when one sublattice has a large offset, and effectively is depleted of all particles. More interesting is the case where one sublattice is nearly in a Mott state, with an integer number of particles per site, while the other is in a robust superfluid state, with large number fluctuations. We explain how such phenomena can be measured in experiments.

II. MODEL

We consider bosons hopping on a lattice with two different types of sites, A and B. We will mostly be thinking about two-dimensional examples, but the formalism also applies to higher dimensions. Extensions to more sublattices are straightforward, and most of the structure is clear from the two-sublattice case.

Generically there will be terms in the Hamiltonian which involve A sites, terms involving B sites, and those that connect the two sublattices. We will take the interactions to be strictly local, as is appropriate for most cold-gas experiments. Thus we write $\mathcal{H} = \mathcal{H}_A + \mathcal{H}_B + \mathcal{H}_{AB}$ with

$$\mathcal{H}_A = \sum_{i\in A}\left(\frac{U_A}{2}a_i^\dagger a_i^\dagger a_i a_i - \mu_A a_i^\dagger a_i\right) - t_A\sum_{\substack{\langle i,j\rangle\\ i,j\in A}}(a_i^\dagger a_j + a_j^\dagger a_i),$$

$$\mathcal{H}_B = \sum_{i\in B}\left(\frac{U_B}{2}b_i^\dagger b_i^\dagger b_i b_i - \mu_B b_i^\dagger b_i\right) - t_B\sum_{\substack{\langle i,j\rangle\\ i,j\in B}}(b_i^\dagger b_j + b_j^\dagger b_i),$$

$$\mathcal{H}_{AB} = -t_{AB}\sum_{\substack{\langle i,j\rangle\\ i\in A,\, j\in B}}(a_i^\dagger b_j + b_j^\dagger a_i), \tag{1}$$

where $a_i^\dagger$ and a_i are the creation and annihilation operators for the A sites, $b_i^\dagger$ and b_i are those for B sites, and $\langle i, j\rangle$ denotes

*as2755@cornell.edu
†em256@cornell.edu

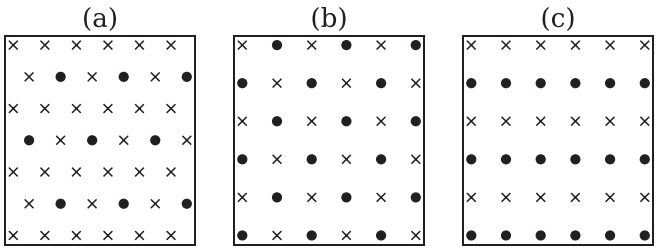

FIG. 1. Example lattices: (a) kagome; (b) checkerboard; (c) stripe. In all cases the local potential is different on the A sublattice, marked by x's, and the B sublattice, marked by dots.

neighbors. The coefficients t_A, t_B, t_{AB} are hopping matrix elements, U_A, U_B are on-site interactions, and μ_A, μ_B represent the chemical potentials of the two sublattices. In particular, for the experiments we are considering $\mu_B = \mu_A + V$, where V is the energy offset. Models of this form have been referred to as *ionic* Bose Hubbard models [34,35].

The relevance of the various terms depends on the lattice geometry. For example, the kagome lattice in Fig. 1(a) has no B-B neighbors, while the checkerboard lattice in Fig. 1(b) has neither A-A neighbors nor B-B neighbors.

The sublattices do not need to have simple Bravais structures, but in all our examples the sites in each unit cell will be symmetry related. For example, the A sites in the kagome lattice [the x's in Fig. 1(a)] have a three-site basis, but are all equivalent. Generalizing to more complicated structures is straightforward.

As explained by Fisher *et al.* [36], the principle features of Bose-Hubbard models such as Eq. (1) are captured by the variational ansatz,

$$|\psi\rangle = \left(\bigotimes_{i\in A}\sum_n f_n^A|n\rangle_i\right)\left(\bigotimes_{i\in B}\sum_n f_n^B|n\rangle_i\right), \tag{2}$$

where $|n\rangle_i$ is the Fock state with n particles at site i. We characterize the ground state by minimizing $\langle\mathcal{H}\rangle = \langle\psi|\mathcal{H}|\psi\rangle$, treating the f_n^σ as variational parameters, with the normalization constraint $\sum_n |f_n^\sigma|^2 = 1$.

The order parameters for superfluidity in each sublattice are

$$\alpha \equiv \langle a_i\rangle = \sum_n \sqrt{n}\, f_{n-1}^A \left(f_n^A\right)^*,$$
$$\beta \equiv \langle b_i\rangle = \sum_n \sqrt{n}\, f_{n-1}^B \left(f_n^B\right)^*. \tag{3}$$

The hopping in $\mathcal{H}_{AB}$ couples these order parameters, so that, if one of these is nonzero, then so is the other. More formally, $\langle\mathcal{H}\rangle$ contains a term proportional to $\alpha\beta$, implying that the only stationary point of the energy with $\alpha = 0$ also has $\beta = 0$. This feature can be interpreted as a "proximity effect"—superfluidity on one sublattice induces superfluidity on the other.

III. RESULTS

As detailed in Appendix A, we numerically minimize the energy as a function of the parameters in Eq. (1). In addition to superfluid phases, where α and β are nonzero, we find insulator phases with $\alpha = \beta = 0$. These are incompressible phases with an integer number of particles n_A, n_B on the sites of each sublattice. Figure 2 shows representative phase diagrams taking parameters corresponding to the kagome lattice shown in Fig. 1. We take all hopping matrix elements equal to one another, $t_A = t_B = t_{AB} = t$, but for this lattice there are no nearest-neighbor sites on the B sublattice, so t_B does not matter. Similarly, we take the interactions to be equal $U_A = U_B = U$. We vary μ_A and the offset $V = \mu_B - \mu_A$.

When $V = 0$ this geometry reduces to a simple triangular lattice. The Mott lobes have $n_A = n_B$ and the order parameters on the two sublattices are identical [Fig. 2(a)]. For small V the lobes split: n_A and n_B increment independently [Fig. 2(b)]. When $V > U$, there will be multiple lobes where $n_B = 0$ [Fig. 2(c)].

In addition to showing phase boundaries, in Fig. 2 we plot the surfaces of fixed condensate density, $|\alpha|^2$ and $|\beta|^2$. As is evident in Fig. 2(b), there are regions where one order parameter is much bigger than the other. These regions are found between pairs of lobes, and alternate: when n_A increments, one finds $|\alpha|^2 \gg |\beta|^2$, and vice versa when n_B increments. One interpretation of this asymmetry is that it is a manifestation of the proximity effect [37]: between two lobes where n_B is unchanged, the B sublattice is nearly a Mott insulator, and it is only proximity to the A superfluid which makes the order parameter nonzero.

Another feature of Fig. 2 is that the lobes where n_A increment have larger gaps between them than those where n_B increment. This is due to the fact that there are no B-B neighbors, making the B superfluid less stable. Figure 3 shows the phase boundaries for the stripe lattice, where the two sublattices are equivalent. There we see much more even spacing between the lobes.

In Fig. 4, we plot the densities as a function of μ_A for fixed t. This corresponds to a vertical slice through the phase diagram. One sees a series of plateaus, corresponding to the insulating states. The two densities increment sequentially. Notice that the density of one of the sublattices is nearly uniform in the superfluid region between two lobes. Thus the fluid on that sublattice is approximately incompressible. As apparent in the inset, if one zooms in, one can find some variation of the density in these regions. Interestingly the slope $\partial\langle n_\sigma\rangle/\partial\mu_A$ can even be slightly negative, but the total compressibility $\partial\langle n_A + n_B\rangle/\partial\mu_A$ is always positive.

Figure 5 illustrates the behavior of the order parameters as a function of t/U for several fixed values of μ_A/U. This corresponds to horizontal slices through the phase diagram. Figure 5(a) shows a slice between lobes where $(n_a, n_b) = (1, 0)$ and (1,1). The A-lattice order parameter becomes extremely small as $t \to 0$, while the B-lattice order parameter approaches a constant. Figure 5(c) shows the opposite case. Figure 5(b) shows the generic case, where one has an insulator at small t. For these parameters one is on the part of the lobe which is near the (1,1) to (2,1) transition, and hence $|\alpha|^2 > |\beta|^2$. In this generic case the condensate densities vanish linearly as one approaches the Mott lobe.

An intuitive way of understanding all of this structure is to simply take two copies of the phase diagram in Fig. 2(a), which represent each of the two sublattices. One of the phase diagrams is displaced vertically by V, and the regions where

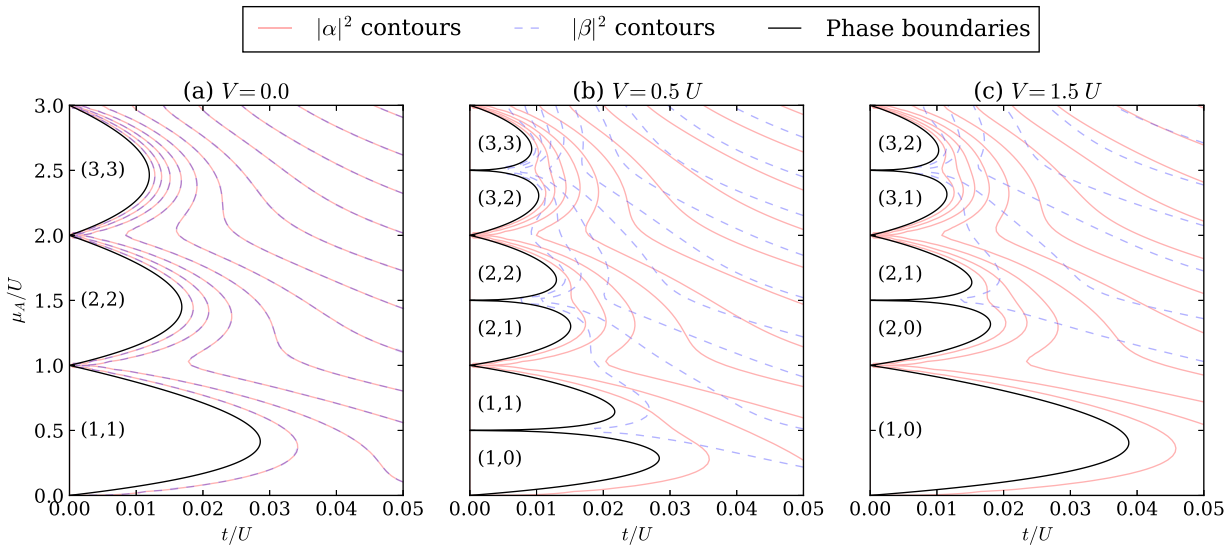

FIG. 2. Phase boundaries for the kagome lattice for three different values of the sublattice bias V. Energies are given in terms of the on-site interaction U. Mott states with n_A and n_B atoms per site on each sublattice are labeled by (n_A, n_B). Solid (red) curves and dashed (blue) curves denote evenly spaced contours of fixed condensate densities, $|\alpha|^2$ and $|\beta|^2$, with spacing 0.25.

the Mott lobes overlap become the Mott lobes of the combined system. The regions where only one of the sublattices has Mott lobes develops superfluidity due to the proximity effect. Note, this intuitive construction only qualitatively captures the shapes of the Mott lobes.

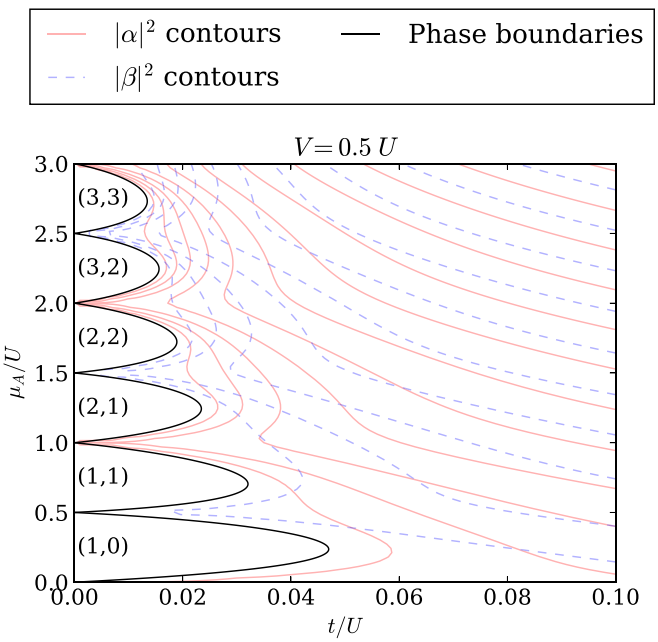

FIG. 3. Phase boundaries for the striped lattice with sublattice bias $V = 0.5$. Energies are given in terms of the on-site interaction U. Mott states with n_A and n_B atoms per site on each sublattice are labeled by (n_A, n_B). Solid (red) curves and dashed (blue) curves denote evenly spaced contours of fixed condensate densities, $|\alpha|^2$ and $|\beta|^2$, with spacing 0.25. In contrast to the kagome lattice, for the striped lattice the lobes are more symmetric.

IV. EXPERIMENTAL DETECTION

A key question is how the sublattice superfluidity will manifest in an experiment. The order parameters $|\alpha|^2$ and $|\beta|^2$ correspond to macroscopic occupation of $k = 0$ states in each sublattice, and will therefore lead to sharp peaks in time-of-flight expansion [38]. For the kagome lattice, the condensate contribution to the time-of-flight image is a series of peaks which again form a kagome lattice, with the dots and x's in Fig. 1 having intensities proportional to $|3\alpha + \beta|^2$ and $|\alpha - \beta|^2$. Thus, by comparing the intensities of the Bragg peaks, one can extract the ratios of the condensate fractions. The full argument is given in Appendix C.

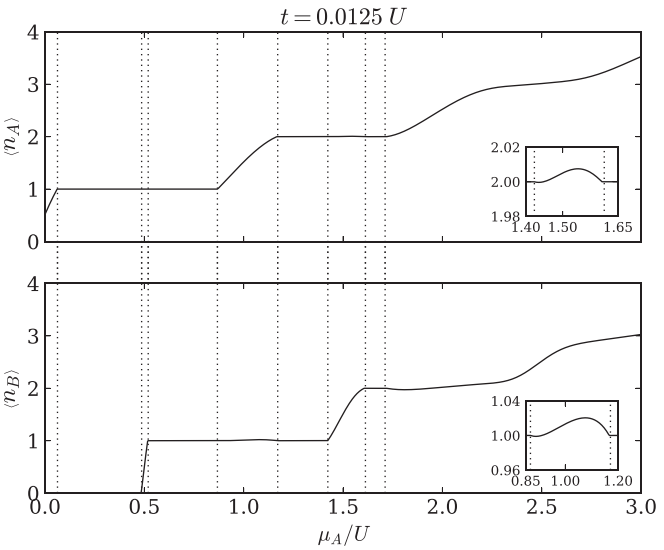

FIG. 4. Densities on two sublattices of the kagome lattice for $V = 0.5U$ and $t = 0.0125U$ [see Fig. 2(b)]. Dotted vertical lines show phase boundaries. Insets show magnified views, with the same axes.

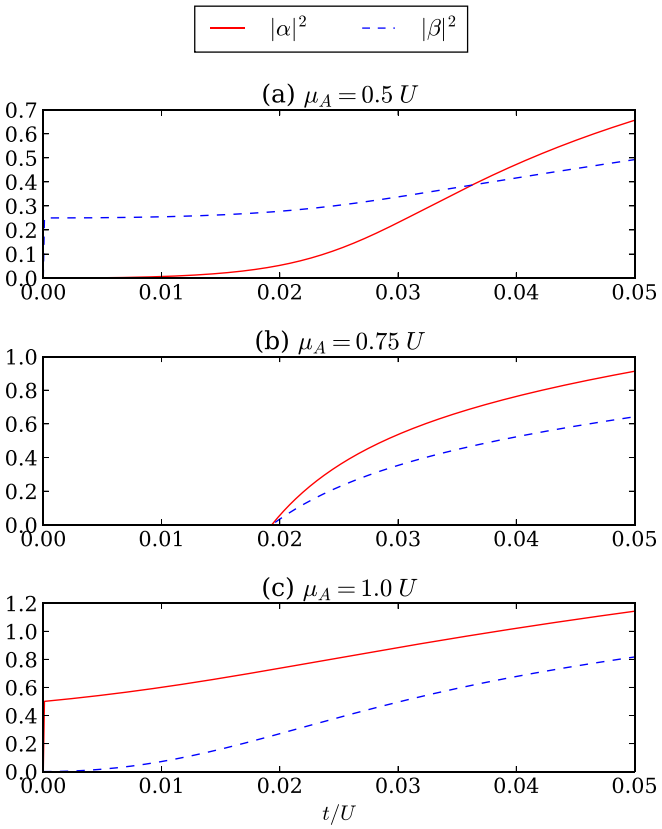

FIG. 5. Order parameters on two sublattices of the kagome lattice for $V = 0.5U$ and (a) $\mu_A = 0.5U$, (b) $\mu_A = 0.75U$, and (c) $\mu_A = U$. Solid (red) and dashed (blue) curves correspond to $|\alpha|^2$ and $|\beta|^2$.

An alternative probe is site-resolved *in situ* imaging [39], which can measure the densities n_A and n_B. In principle one could thereby identify the Mott states. As illustrated in Fig. 4, there are however regions of parameter space in which the superfluid has nearly an integer number of particles per site. These regions may make it difficult to use *in situ* imaging to find the phase boundaries. Achieving the required precision may also be challenging.

Another option for detecting the density differences between sublattices is light scattering. This technique has been used to find antiferromagnetic spin correlations [40].

V. SUMMARY

We have studied the influence of sublattice bias on the superfluid to insulator transition of a Bose gas in an optical lattice. Within the Gutzwiller mean-field theory, superfluidity on one sublattice is always accompanied by superfluidity on the other. The Mott lobes are characterized by integer densities on each sublattice. These increment sequentially as the chemical potential is increased. Between the lobes there are regions where one superfluid density is much larger than the other. These features are observable through *in situ* and time-of-flight probes.

Our most nontrivial result is the rich structure of the condensate density on the two sublattices. As experimental lattice geometries become ever-more sophisticated, these considerations will become more and more important. Crucially, these biased lattices are a promising platform for searching for more exotic physics. For example, related geometries have been used to study fractional Mott insulators [41,42].

ACKNOWLEDGMENTS

This material is based upon work supported by the National Science Foundation (US) under Grant No. PHY-1508300.

APPENDIX A: MINIMIZING THE ENERGY

Within our variational theory, the energy $\langle\mathcal{H}\rangle$ is a quartic form in the coefficients f_n^σ and their complex conjugates, where $\sigma = A, B$ labels the sublattice. The quartic terms are products of the mean fields $\psi^A \equiv \alpha$ and $\psi^B \equiv \beta$, and their complex conjugates. This feature, combined with the relation $\partial\psi^\sigma/\partial(f_n^\sigma)^* = \sqrt{n} f_{n-1}^\sigma$, means that the derivative $\partial\langle\mathcal{H}\rangle/\partial(f_n^\sigma)^*$ has a simple form. Making $\langle H\rangle$ stationary, with the constraint $\langle\psi||\psi\rangle = 1$, yields a set of cubic equations that can be written

$$\Lambda_n^\sigma f_n^\sigma + \Gamma_{n+1}^\sigma f_{n+1}^\sigma + \Gamma_n^{\sigma^*} f_{n-1}^\sigma = \lambda^\sigma f_n^\sigma, \tag{A1}$$

where $\sigma, \tau \in \{A, B\}$, and

$$\Lambda_n^\sigma = \frac{N_\sigma}{2} n(n-1) - N_\sigma \frac{\mu_\sigma}{U} n, \tag{A2}$$

$$\Gamma_n^\sigma = \sum_\tau \left(-\frac{t_{\sigma\tau}}{U}\right)(N_\sigma s_{\sigma\tau}\sqrt{n}\ \psi^\tau). \tag{A3}$$

Here N_σ is the number of sites in sublattice σ and $s_{\sigma\tau}$ is the number of τ neighbors of each σ site. Λ is independent of the f's, while Γ depends on the f's only through ψ.

The cubic eigenvalue equation in Eq. (A1) can be solved efficiently by an iterative method. We start with a guess for ψ^τ in Eq. (A2). We then solve Eq. (A1) as a linear eigenvalue equation. That solution is then used to update ψ^τ. Both the time for each iteration and the total number of iterations needed for convergence are favorable.

APPENDIX B: PHASE BOUNDARIES

The Mott insulator regions in the $\frac{\mu}{U}$-$\frac{t}{U}$ parameter space can be labeled by integers $n_A = \langle a_i^\dagger a_i\rangle$ and $n_B = \langle b_i^\dagger b_i\rangle$. Consider a point in the superfluid region infinitesimally close to the insulator region with $n_A = j$, $n_B = k$. To the leading order, we must have

$$f_{j-1}^A = \epsilon_-, \qquad f_{k-1}^B = \eta_-,$$
$$f_{j+1}^A = \epsilon_+, \qquad f_{k+1}^B = \eta_+,$$
$$f_j^A = \sqrt{1-\epsilon_-^2-\epsilon_+^2}, \qquad f_k^B = \sqrt{1-\eta_-^2-\eta_+^2}.$$

All the other f's vanish. As we approach the insulator, the parameters $\{\epsilon, \eta\}$ become smaller, vanishing at the phase boundary. Consequently, we can expand the energy as

$$\langle H\rangle = (\epsilon_+ \quad \epsilon_- \quad \eta_+ \quad \eta_-) M \begin{pmatrix} \epsilon_+ \\ \epsilon_- \\ \eta_+ \\ \eta_- \end{pmatrix} + \cdots,$$

where M is a 4×4 matrix and, in addition to a constant, the neglected terms contain higher powers of the small parameters. The phase transition is characterized by $\det(M) = 0$, as M is positive definite in the insulating phase, but has at least one negative eigenvalue in the superfluid phase. This equation gives the phase transition boundary in the $\frac{\mu}{U}$-$\frac{t}{U}$ parameter space.

The equation $\det(M) = 0$ can be factored as the product of two quadratic equations in t which have closed form solutions. These analytic expressions are not particularly enlightening.

APPENDIX C: TIME OF FLIGHT

As explained in the main text, the time-of-flight density pattern can reveal the sublattice condensate fraction. Here we calculate this pattern for a kagome lattice with sublattice bias.

The time-of-flight image from a lattice gas contains two components: a diffuse background from the noncondensed particles and sharp Bragg peaks from the condensate. Here we solely consider the latter, which are readily distinguished. As explained in [38], the asymptotic profile is simply given by the Fourier transform of the *in situ* condensate wave function, $\psi(\mathbf{k}, t) \propto \psi_{\mathbf{k}=\frac{m\mathbf{r}}{t}}$, where $\psi_{\mathbf{k}} = \int d\mathbf{r}\; e^{-i\mathbf{k}\cdot\mathbf{r}}\psi(\mathbf{r}, 0)$.

The initial state of the system can be written as

$$\psi(\mathbf{r}, 0) = \sum_{i\in A} \alpha\phi(\mathbf{r} - \mathbf{r_i}) + \sum_{i\in B} \beta\phi(\mathbf{r} - \mathbf{r_i}), \tag{C1}$$

with the Fourier transform,

$$\psi_{\mathbf{k}}(0) = \sum_{i\in A} \alpha\, e^{-i\mathbf{k}\cdot\mathbf{r}_i}\phi_{\mathbf{k}} + \sum_{i\in B} \beta\, e^{-i\mathbf{k}\cdot\mathbf{r}_i}\phi_{\mathbf{k}}, \tag{C2}$$

where $\phi_{\mathbf{k}}$ is the Fourier transform of the Wannier state $\phi(\mathbf{r})$.

The sites in sublattice A belong to one of three Bravais lattices $\mathbf{r}_s = m\mathbf{u} + n\mathbf{v} + \delta_s$, where $\mathbf{u} = (a, 0)$, $\mathbf{v} = (a\cos\frac{\pi}{3}, a\sin\frac{\pi}{3})$, m and n are integers, and δ_s takes on one of three values: $\delta_0 = (0, 0)$, $\delta_1 = \mathbf{u}/2$, or $\delta_2 = \mathbf{v}/2$. The sites in sublattice B belong to the Bravais lattice $\mathbf{r}_3 = m\mathbf{u} + n\mathbf{v} + \delta_3$, with $\delta_3 = (\mathbf{u} + \mathbf{v})/2$. Then, we can write

$$\begin{aligned}\sum_{i\in A} e^{-i\mathbf{k}\cdot\mathbf{r}_i} &= F(\mathbf{k})\left(1 + e^{-i\mathbf{k}\cdot\frac{\mathbf{u}}{2}} + e^{-i\mathbf{k}\cdot\frac{\mathbf{v}}{2}}\right),\\ \sum_{i\in B} e^{-i\mathbf{k}\cdot\mathbf{r}_i} &= F(\mathbf{k})\, e^{-i\mathbf{k}\cdot(\frac{\mathbf{u}}{2}+\frac{\mathbf{v}}{2})},\end{aligned} \tag{C3}$$

where $F(\mathbf{k}) = \sum_{m,n} e^{-i\mathbf{k}\cdot(m\mathbf{u}+n\mathbf{v})}$ is zero unless $\mathbf{k}\cdot(m\mathbf{u} + n\mathbf{v})$ is a multiple of 2π for all integers m, n. We define reciprocal lattice vectors $\mathbf{k}_1, \mathbf{k}_2$ such that $\mathbf{k}_1\cdot\mathbf{u} = 2\pi$, $\mathbf{k}_1\cdot\mathbf{v} = 0$, $\mathbf{k}_2\cdot\mathbf{u} = 0$, and $\mathbf{k}_2\cdot\mathbf{v} = 2\pi$. In particular, $\mathbf{k}_1 = (\frac{2\pi}{a}, -\frac{2\pi}{a}\cot\frac{\pi}{3})$, $\mathbf{k}_2 = (0, \frac{2\pi}{a}\csc\frac{\pi}{3})$ are the basis for a triangular lattice. Standard analysis gives $F(\mathbf{k}) \propto \sum_{m,n}\delta(\mathbf{k} - m\mathbf{k}_1 - n\mathbf{k}_2)$.

Because of coherence factors in Eq. (C3), the number of atoms in the peak at position $\mathbf{r}_{mn} = \frac{t}{m}(m\mathbf{k}_1, n\mathbf{k}_2)$ is

$$N_{nm} \propto |\alpha[1 + (-1)^n + (-1)^m] + \beta(-1)^{n+m}|^2|\phi_{nm}|^2, \tag{C4}$$

where $\phi_{nm} = \phi_{\mathbf{k}}$ at $\mathbf{k} = m\mathbf{r}/t$. Neglecting this slow envelope yields

$$\begin{aligned}N_{00} = N_{22} &\propto |3\alpha + \beta|^2,\\ N_{11} = N_{10} = N_{01} &\propto |\alpha - \beta|^2.\end{aligned} \tag{C5}$$

[1] M. Greiner, O. Mandel, T. Esslinger, T. W. Hänsch, and I. Bloch, Nature (London) **415**, 39 (2002).
[2] B. DeMarco, C. Lannert, S. Vishveshwara, and T.-C. Wei, Phys. Rev. A **71**, 063601 (2005).
[3] G. K. Campbell, Science **313**, 649 (2006).
[4] S. Fölling, A. Widera, T. Müller, F. Gerbier, and I. Bloch, Phys. Rev. Lett. **97**, 060403 (2006).
[5] F. Gerbier, A. Widera, S. Fölling, O. Mandel, T. Gericke, and I. Bloch, Phys. Rev. A **72**, 053606 (2005).
[6] F. Gerbier, A. Widera, S. Fölling, O. Mandel, T. Gericke, and I. Bloch, Phys. Rev. Lett. **95**, 050404 (2005).
[7] C. Orzel, Science **291**, 2386 (2001).
[8] Z. Hadzibabic, S. Stock, B. Battelier, V. Bretin, and J. Dalibard, Phys. Rev. Lett. **93**, 180403 (2004).
[9] C. Schori, T. Stöferle, H. Moritz, M. Köhl, and T. Esslinger, Phys. Rev. Lett. **93**, 240402 (2004).
[10] K. Xu, Y. Liu, D. E. Miller, J. K. Chin, W. Setiawan, and W. Ketterle, Phys. Rev. Lett. **96**, 180405 (2006).
[11] P. Sengupta, M. Rigol, G. G. Batrouni, P. J. H. Denteneer, and R. T. Scalettar, Phys. Rev. Lett. **95**, 220402 (2005).
[12] T. Stöferle, H. Moritz, C. Schori, M. Köhl, and T. Esslinger, Phys. Rev. Lett. **92**, 130403 (2004).
[13] F. Gerbier, S. Fölling, A. Widera, O. Mandel, and I. Bloch, Phys. Rev. Lett. **96**, 090401 (2006).
[14] W. S. Bakr, A. Peng, M. E. Tai, R. Ma, J. Simon, J. I. Gillen, S. Folling, L. Pollet, and M. Greiner, Science **329**, 547 (2010).
[15] G.-B. Jo, J. Guzman, C. K. Thomas, P. Hosur, A. Vishwanath, and D. M. Stamper-Kurn, Phys. Rev. Lett. **108**, 045305 (2012).
[16] S. S. Natu, E. J. Mueller, and S. Das Sarma, Phys. Rev. A **93**, 063610 (2016).
[17] D. S. Goldbaum and E. J. Mueller, Phys. Rev. A **77**, 033629 (2008).
[18] R. O. Umucalılar and M. O. Oktel, Phys. Rev. A **76**, 055601 (2007).
[19] R. O. Umucalılar and E. J. Mueller, Phys. Rev. A **81**, 053628 (2010).
[20] C. K. Thomas, T. H. Barter, T.-H. Leung, M. Okano, G.-B. Jo, J. Guzman, I. Kimchi, A. Vishwanath, and D. M. Stamper-Kurn, Phys. Rev. Lett. **119**, 100402 (2017).
[21] C. Becker, P. Soltan-Panahi, J. Kronjäger, S. Dörscher, K. Bongs, and K. Sengstock, New J. Phys. **12**, 065025 (2010).
[22] P. Soltan-Panahi, J. Struck, P. Hauke, A. Bick, W. Plenkers, G. Meineke, C. Becker, P. Windpassinger, M. Lewenstein, and K. Sengstock, Nat. Phys. **7**, 434 (2011).
[23] S. Taie, H. Ozawa, T. Ichinose, T. Nishio, S. Nakajima, and Y. Takahashi, Sci. Adv. **1**, 1500854 (2015).
[24] P. Windpassinger and K. Sengstock, Rep. Prog. Phys. **76**, 086401 (2013).
[25] L. Tarruell, D. Greif, T. Uehlinger, G. Jotzu, and T. Esslinger, Nature (London) **483**, 302 (2012).
[26] T. H. Barter, T.-H. Leung, M. Okano, M. Block, N. Y. Yao, and D. M. Stamper-Kurn, Phys. Rev. A **101**, 011601(R) (2020).

[27] G. Wirth, M. Ölschläger, and A. Hemmerich, Nat. Phys. **7**, 147 (2011).
[28] H.-N. Dai, B. Yang, A. Reingruber, H. Sun, X.-F. Xu, Y.-A. Chen, Z.-S. Yuan, and J.-W. Pan, Nat. Phys. **13**, 1195 (2017).
[29] S. Nascimbène, Y.-A. Chen, M. Atala, M. Aidelsburger, S. Trotzky, B. Paredes, and I. Bloch, Phys. Rev. Lett. **108**, 205301 (2012).
[30] G. Roati, C. D'Errico, L. Fallani, M. Fattori, C. Fort, M. Zaccanti, G. Modugno, M. Modugno, and M. Inguscio, Nature (London) **453**, 895 (2008).
[31] M. White, M. Pasienski, D. McKay, S. Q. Zhou, D. Ceperley, and B. DeMarco, Phys. Rev. Lett. **102**, 055301 (2009).
[32] L. Guidoni, C. Triché, P. Verkerk, and G. Grynberg, Phys. Rev. Lett. **79**, 3363 (1997).
[33] M. Di Liberto, T. Comparin, T. Kock, M. Ölschläger, A. Hemmerich, and C. M. Smith, Nat. Commun. **5**, 5735 (2014).
[34] M. Messer, R. Desbuquois, T. Uehlinger, G. Jotzu, S. Huber, D. Greif, and T. Esslinger, Phys. Rev. Lett. **115**, 115303 (2015).
[35] J. Hubbard and J. B. Torrance, Phys. Rev. Lett. **47**, 1750 (1981).
[36] M. P. A. Fisher, P. B. Weichman, G. Grinstein, and D. S. Fisher, Phys. Rev. B **40**, 546 (1989).
[37] H. Meissner, Phys. Rev. **117**, 672 (1960).
[38] M. Lewenstein, A. Sanpera, and V. Ahufinger, *Ultracold Atoms in Optical Lattices* (Oxford University Press, Oxford, 2012).
[39] S. Kuhr, Natl. Sci. Rev. **3**, 170 (2016).
[40] T. A. Corcovilos, S. K. Baur, J. M. Hitchcock, E. J. Mueller, and R. G. Hulet, Phys. Rev. A **81**, 013415 (2010).
[41] Q.-H. Chen, P. Li, and H. Su, J. Phys.: Condens. Matter **28**, 256001 (2016).
[42] P. Buonsante, V. Penna, and A. Vezzani, Phys. Rev. A **72**, 031602(R) (2005).